

Chandra Observations of the Nucleus of M33

Guillaume Dubus and Robert E. Rutledge
California Institute of Technology, MS 130-33, Pasadena, CA 91125, U.S.A.

March 2002

ABSTRACT

The nearby galaxy M33 hosts the most luminous steady X-ray source in the Local Group. The high spatial resolution of *Chandra* allows us to confirm that this ultra-luminous X-ray source is within the nucleus and rule out at the 4.6σ level a previously proposed possible counterpart located $1''$ away. The X-ray spectrum is well fitted by a disc blackbody with $kT_{\text{in}} = 1.18 \pm 0.02$ keV and $R_{\text{in}}(\cos \theta)^{0.5} = 57 \pm 3$ km, consistent with earlier results from *ASCA* and *BeppoSAX*. The source flux is steady between 1 and 10^4 s ($< 3\%$ rms variability, 0.5–10 keV) with a 0.5–10 keV luminosity of 1.5×10^{39} erg s $^{-1}$. The X-ray properties and an association with a radio source are reminiscent of the galactic microquasar GRS 1915+105.

Key words: galaxies: individual (M33) — galaxies: nuclei — Local Group — X-rays: galaxies.

1 INTRODUCTION

The nearby galaxy M33 ($d \approx 795$ kpc; van den Bergh 1991) hosts the most luminous steady X-ray source in the Local Group. M33 X-8 dominates the X-ray emission from the galaxy with a 1–10 keV luminosity of about $1.2 \cdot 10^{39}$ erg s $^{-1}$, ten times more than that of the other X-ray sources in the field. The ultra-luminous X-ray source (ULX) has been detected at this level since its discovery by *Einstein*. (Long et al. 1981; Markert & Rallis 1983; Gottwald et al. 1987; Peres et al. 1989; Takano et al. 1994; Long et al. 1996; Parmar et al. 2001). Observations obtained with the *ROSAT* High Resolution Imager (HRI) showed that X-8 is point-like and coincident with the optical nucleus of M33 at the HRI $5''$ resolution (Schulman & Bregman 1995). These also revealed a 106 day $\sim 20\%$ modulation of the X-ray flux from M33 X-8 (Dubus et al. 1997).

The nature of the X-ray emitting object is rather puzzling. The measured velocity dispersion of the nucleus places an upper limit of $1500 M_{\odot}$ on the mass of a putative massive central black hole (Gebhardt et al. 2001). A low luminosity active galactic nucleus (AGN) is therefore unlikely. Indeed, the UV/optical spectrum of the nucleus shows no signs of AGN-type activity and is best modelled by a combination of two starbursts at 40 Myrs and 1 Gyr (Long, Charles & Dubus 2002 and references therein).

The 106 day modulation suggests a single object is responsible for most of the X-ray emission, perhaps a persistent X-ray binary with a $10 M_{\odot}$ black hole radiating at the Eddington luminosity. *Hubble Space Telescope* observations place a limit of 18% on the contribution of a point source to the total far-UV flux from the nucleus (Dubus et al. 1999b). The implied ratio $L_{\text{opt}}/L_X \sim 0.05$ would be in line with expectations from a low-mass X-ray binary. The counterpart would then be mostly lost in the glare of the nucleus. However, there remains a distinct possibility that M33 X-8 is associated with a UV bright star located $1''$ to the NNW (Dubus et al. 1999b). The star has a O9III spectrum with no outstanding

Table 1. *Chandra* Observations of M33

Det.	ObsId	Seq.#	Date	Exp.	offset
ACIS-I	1730	600145	7/12/2000	49.4 ks	0'
ACIS-S	786	600089	8/30/2000	46.2 ks	0'
ACIS-S	787	600090	1/11/2000	9.2 ks	7.7'

Det. is the detector used; exp. is the total integration time; offset is the distance of M33 X-8 from the telescope axis. The CCD frame time was 3.2 s for the first two observations and 1.0 s for the last, offset observation.

feature linking it to the powerful X-ray source but cannot be ruled out at the *ROSAT* HRI resolution (Long, Charles & Dubus 2002).

Most studies have assumed M33 X-8 is associated with the nucleus and used this to register the X-ray images. *Chandra* offers the opportunity to locate M33 X-8 to unprecedented accuracy and settle whether this source is within the nucleus or not. Three observations of M33 are available in the *Chandra* archive (Table 1). We used the first two to accurately position M33 X-8 with respect to *HST* Planetary Camera (PC) images of the nucleus (§2). The third, non piled-up observation is used to study the X-ray spectrum and timing behaviour of M33 X-8 (§3 and §4). Our results are discussed in the last section.

2 ASTROMETRY

The 1–2'' precision of the *Chandra* pipeline aspect solution¹ is insufficient for our purposes. To improve on this, we identified X-ray sources within the field-of-view and cross-correlated these to optical, IR and radio sources with accurately known positions.

¹ <http://cxc.harvard.edu/cal/ASPECT/celmon/index.html>

2.1 X-ray position of the nucleus

M33 X-8 is severely affected by pile-up in the two 50 ks ACIS observations. The count rate in the ACIS-S observation is 0.5 counts/frame compared to 3.0 counts/frame in the 10 ks non piled-up 10 ks ACIS-S observation (see §3 below). The pile-up fraction is therefore about 84% which makes it impossible to study the radial extension of the source to higher accuracy than the *ROSAT* HRI. Observations with the *Chandra* HRC would be able to resolve any contribution from extended emission or faint point sources within $5''$. The inner pixels of the ACIS-S (Fig. 1) are very piled-up hence have a dearth of counts so that the 0.5-2 keV image is doughnut shaped (standard G02346 events). Going to higher energies reduces the effect and there is a very well defined peak in both ACIS-S and I.

CELLDETECT (CIAO v2.2.0.1²) locates M33 X-8 at $(4098.1, 4057.2) \pm 0.1$ pixels in the ACIS-I and at $(4063.0, 4026.3) \pm 0.5$ pixels in the ACIS-S. To check these values, we redefined the center as the location which minimizes the distances of all the events within a 300 pixel wide box roughly centered on M33 X-8 (this assumes circular symmetry and avoids the problem posed by a pile-up doughnut). The values obtained by selecting only the events with energies above 1, 2 or 5 keV are all consistent with the CELLDETECT locations and errors which we therefore adopt.

2.2 Optical position of the nucleus

The optical position of the nucleus we adopt is the 2MASS position which is tied to the Tycho reference frame. The (compact) nucleus is detected with $J = 12.08 \pm 0.04$ in this survey. At α (J2000) $1^{\text{h}}33^{\text{m}}50^{\text{s}}.89$ and δ $30^{\circ}39'36''.75$ with an uncertainty of $0''.15$ this is, as far as we know, the best available absolute position. The position of the close O9III star was then found relative to the nucleus using the UV *HST* PC image described in Dubus et al. (1999b). We find α $1^{\text{h}}33^{\text{m}}50^{\text{s}}.85$ and δ $30^{\circ}39'37''.65$ to the 2MASS uncertainty.

As an independent check, we cross-correlated the brightest stars in the various *HST* PC images of the nucleus (Dubus et al. 1999b) with the M33 star catalogue produced by the DIRECT project (Macri et al. 2001a). The DIRECT positions are tied to the USNO-A2 reference frame with an accuracy of $0''.4$ - $0''.7$. We found 4-6 stars (depending upon the sky orientation of the PC chip) that correlated well with DIRECT positions, all lying at the same offset within $0''.1$ - $0''.4$ of each other. We found a mean corrected position for the nucleus of α $1^{\text{h}}33^{\text{m}}50^{\text{s}}.90$ and δ $30^{\circ}39'37''.14$. This is consistent with the 2MASS position within the limits of the DIRECT astrometric solution.

2.3 X-ray source list and cross-correlation

We applied CELLDETECT to identify X-ray sources in the two 50 ks observations. The detection threshold was 4σ , resulting in 51 (77) possible sources in the ACIS-I (ACIS-S) dataset. We compared this list with the *ROSAT* X-ray catalogue of Haberl & Pietsch (2001) to identify previously known X-ray sources. *ROSAT* and *Chandra* sources lying within $5''$ of each other were considered identical and are thereafter identified by their number in Table 1 of Haberl & Pietsch (2001).

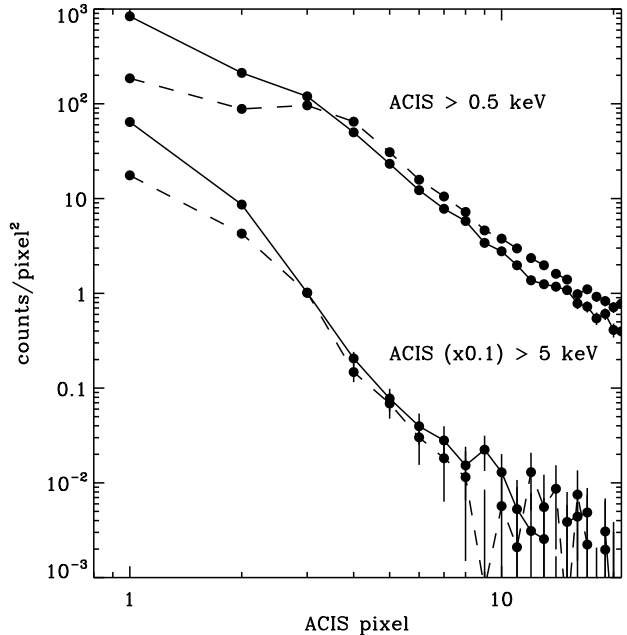


Figure 1. Radial profiles of M33 X-8 in the two piled-up 50 ks ACIS-I (solid lines) and S (dashed line) observations (1 pixel = $0.492''$). All G02346 events with energies > 0.5 keV are used in the top two profiles (9900 and 6600 counts respectively for ACIS-I and S) while only those above 5 keV are used in the bottom profiles (3100 and 1200 counts; profiles are shifted down by a factor 10 for clarity). The profiles are (background subtracted) area-averaged number of events within x and $x-1$ pixels of the adopted centers (§2.1). Pile-up appears most clearly as a flattening of the ACIS-S profile at low energies.

We cross-correlated the X-ray source list with the Tycho-2 (Hog et al. 2000), USNO-A2 (Monet et al. 1998) and 2MASS (Skrutskie et al. 1997) catalogues. We also used a subset (Macri et al. 2001b; Mochejska et al. 2001) of the DIRECT catalogue containing variable optical sources (excluding cepheids) and the radio source catalogue of Gordon et al. (1999). The latter contains optically confirmed supernova remnants (SNR) in M33 and stellar-like background radio sources. The radio positions are accurate with respect to the ICRS frame to $7''/2\sigma$, where $7''$ is the beam size and σ is the signal-to-noise ratio of the source.

We started by searching for all possible counterparts in the catalogues within $10''$ of each X-ray source and plotting their pixel offsets relative to the *Chandra* position. A given X-ray source can be associated with several sources from the same or different catalogues. In the plot, true counterparts will cluster at the offset of the X-ray astrometry (the orientation error and ACIS chip distortion are negligible), while spurious identifications will appear uniformly distributed (the field of view is much greater than the searched correlation radius). The spread of the cluster is a measure of the accuracy of the astrometric solution. There was an obvious concentration of matches around the offset between X-8 and the 2MASS position of the nucleus (Table 2 and Fig. 2). Note that some of the matches may refer to the same object such as the USNO and Tycho match for HP87. None of the DIRECT variable sources matched an X-ray source within $3''$ although we note that a star with a 3.4 days optical period (D33J013334.8+303211.4, Mochejska et al. 2001) lies within $10''$ of the 3.45 day eclipsing X-ray source X-7 (Dubus et al. 1999a).

² <http://cxc.harvard.edu/ciao/>

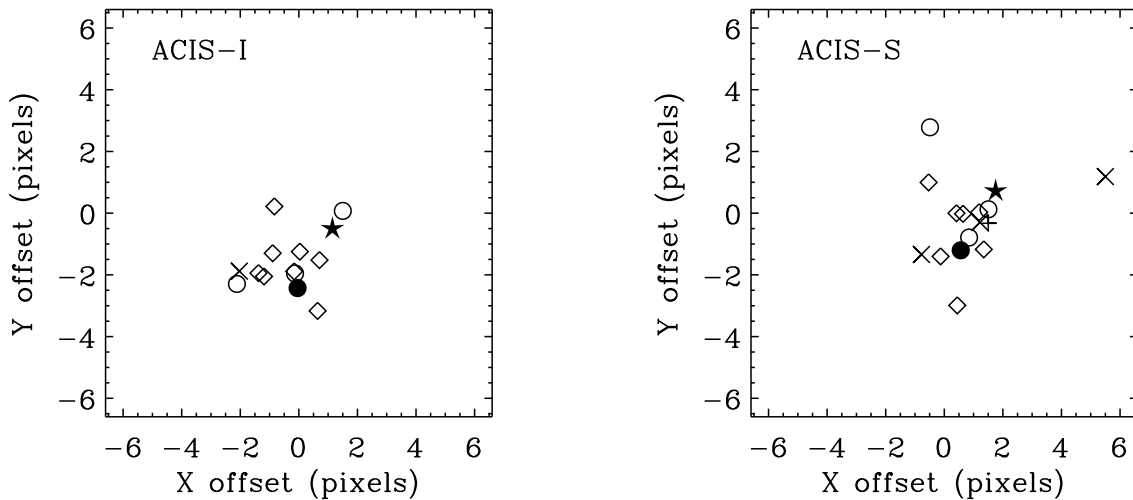


Figure 2. Plot of the offsets in ACIS pixels (1 pixel=0.492'') between X-ray sources and their matches in the USNO (×), Tycho (+), 2MASS (○), and radio (◊, Gordon et al. 1999) catalogues (see Table 1). The offset between the *Chandra* position of X-8 and the 2MASS position of the nucleus is indicated by a ●. The offset between X-8 and the UV bright star ~ 1'' NNW of the nucleus is shown by a ★. The radio counterparts cluster at an offset consistent with the ULX being associated with the nucleus (●) rather than with the nearby star (★).

2.4 Position of the nuclear X-ray source

The clustering of matches around the offset between the 2MASS position of the nucleus and the *Chandra* position of X-8 is particularly clear for the radio correlations (Fig. 2). For uniformly distributed sources, the probability p of having an X-ray source within d arcsec of a possible counterpart is $p \approx (d/D)^2$ if $d \ll D$ and where D is the radius of the field of regard. Correlating N X-ray sources with M possible counterparts in the field of view, the probability P of observing C or more sources within d arcsec of a counterpart is

$$P = 1 - \sum_{i=0}^{C-1} \binom{MN}{i} p^i (1-p)^{MN-i}$$

For $C = 8$ matches with the radio catalogue, $d = 3''$, $N = 32$, $M = 126$ and $D \approx 8'$, the probability of seeing a cluster of 8 associations within $3''$ is $\lesssim 10^{-11}$. The same calculation for the ACIS-S observation ($C = 7$, $N = 57$, $M = 117$) yields a probability $\lesssim 10^{-8}$. We conclude the radio associations are very likely to be true counterparts (in contrast with the USNO, 2MASS and Tycho associations for which the same calculation does not rule out chance superpositions).

We now estimate the probability that the offsets given by the radio counterparts are consistent with the offset between the 2MASS position of the nucleus and X-8 (● in Fig. 2) or the nearby star position and X-8, plotted as a ★ in Fig. 2). A χ^2 test on the measured distances between the radio and nucleus offsets yields a probability 0.28 (0.53) that these are consistent for the ACIS-I (ACIS-S) data. The probability for the radio offsets to be consistent with the nearby star are $2 \cdot 10^{-6}$ (ACIS-I) and $4 \cdot 10^{-4}$ (ACIS-S). The ACIS-S result is less conclusive than the ACIS-I because of the higher uncertainty in the position of X-8 in the ACIS-S (± 0.5 pixel compared to ± 0.1 pixel, see §2.1). We conclude the nearby star is ruled out as a possible counterpart at the 4.6σ level and that M33 X-8 is at the 2MASS position of the nucleus with an uncer-

tainty of $0''.6$ (the mean weighted distance of the radio offsets for both ACIS-I and S).

There is a radio source associated with the nucleus. This source (GDK102) has $F_{20\text{cm}} = 0.6 \pm 0.1$ mJy, $F_{6\text{cm}} = 0.2 \pm 0.1$ mJy is located $0''.6$ away from the 2MASS position (and $0''.4$ away from the mean radio offset) and is a possible counterpart to M33 X-8. Using the results of the above analysis, we note the association of X-ray source HP84 with 2MASS 0133418+303849 ($J = 12.62 \pm 0.02$) is likely to be real. HP84 is classified as a supersoft X-ray source by Haberl & Pietsch (2001).

3 X-RAY SPECTRUM

We performed spectral analysis using data from the ACIS-S observation ObsId 787. We extracted 27259 counts from a circle within $20''$ of the source position for a total of 3.06 counts/frame. The source was $7.7'$ off-axis, at which the the 50% enclosed energy function (EEF) at 1.5 keV is $4''$ vs. $0.3''$ on-axis, resulting in the source covering an area larger by a factor ~ 170 , to 0.02 counts/frame/PSF, at which the estimated pileup fraction should be negligible ($< 1\%$). We confirmed this by comparing the distribution of photon event grades (for grades 0, 2, 3, 4 and 6) below 2 keV and in the 2-8 keV range with those of a non-piled up X-ray observation (of ZW3146, ObsId 1651, Seq. Num 800119) and found that they were roughly consistent, though not identical; however, both were similar to the branching ratio observed from a non piled-up observation of PG1634-706³, and so pileup does not appear to be significant during this observation. Background counts were taken from an annulus of inner- and outer- radii of $25''$ and $100''$. The expected number of background counts in the source region is 167 ± 3 . The background subtracted source countrate is then 2.92 ± 0.02 c/s.

³ <http://asc.harvard.edu/cal/Hrma/hrma/misc/oac/psf2/index.html>

Table 2. All possible matches within $3''$ of X-ray sources (Fig. 2).

Source	Cat.	α (degrees, J2000)	δ	ΔX (pixels)	ΔY (pixels)	err ($''$)
ACIS-I observation (ObsId 1730)						
HP102	2MASS	23.46205	30.66021	-0.0	-2.4	0.16
	GDK102	23.46204	30.66037	0.0	-1.2	0.60
HP84	2MASS	23.42445	30.64703	-0.1	-2.0	0.16
HP74	GDK64	23.39958	30.60785	0.7	-1.5	0.26
HP130	GDK148	23.54462	30.70671	-1.2	-2.1	0.40
HP62	USNO	23.37106	30.70483	-2.0	-1.9	0.19
	GDK50	23.37096	30.70482	-1.4	-1.9	0.42
CXO1	2MASS	23.34009	30.65008	1.5	0.1	0.46
	2MASS	23.34066	30.64976	-2.1	-2.3	0.46
	GDK38	23.34046	30.65010	-0.8	0.2	1.26
HP106	GDK112	23.47858	30.55301	-0.2	-1.9	0.26
HP80	GDK67	23.40621	30.78870	0.6	-3.2	0.52
HP67	GDK57	23.38008	30.55939	-0.9	-1.3	0.27
ACIS-S observation (ObsId 786)						
HP102	2MASS	23.46205	30.66021	0.6	-1.2	0.29
	GDK102	23.46204	30.66037	0.6	-0.0	0.65
HP98	GDK100	23.46025	30.63937	1.3	-1.2	0.25
HP84	2MASS	23.42445	30.64703	0.8	-0.8	0.15
HP62	GDK50	23.37096	30.70482	-0.1	-1.4	0.42
	USNO	23.37106	30.70483	-0.8	-1.3	0.20
HP106	GDK112	23.47858	30.55301	0.4	-0.0	0.22
HP87	Tycho	23.43076	30.77521	1.5	-0.3	0.36
	2MASS	23.43076	30.77527	1.5	0.1	0.38
	USNO	23.43081	30.77521	1.2	-0.3	0.38
	USNO	23.43013	30.77541	5.5	1.2	0.38
CXO2	GDK51	23.37192	30.76057	0.4	-3.0	0.41
HP80	GDK67	23.40621	30.78870	1.2	0.0	0.48
CXO3	2MASS	23.49518	30.83467	-0.5	2.8	0.51
HP64	GDK52	23.37279	30.81954	-0.5	1.0	0.94

HP refers to the Haberl & Pietsch (2001) catalog of ROSAT sources and is used to identify the sources (column 1). CXO refers to *Chandra* sources which were not previously detected. GDK refers to the Gordon et al. (1999) catalog of radio sources in M33 (their Table 1). For each match we list the catalogue (column 2) and position in this catalogue (columns 3 & 4). ΔX and ΔY (columns 5 & 6) are the offsets in ACIS pixels between the X-ray and matched source position (plotted in Fig. 2). Column 5 is the offset error $(\sigma_X^2 + \sigma_{\text{cat}}^2)^{1/2}$, where σ_X^2 is the error in the X-ray source position (given by CELLDetect, see §2.3) and σ_{cat}^2 is the error in the position of the correlated source (given in the relevant catalogue, see §2.3).

Using XSPEC v11.0.1 (Arnaud 1996), we produced a pulse-height-analyser (PHA) spectrum of the extracted counts data between 0.6-9 keV, binning at 130 eV between 0.6 and 2.0 keV, at 260 eV between 2.0 and 5.4 keV, and with two energy bins between 5.4 and 9.0 keV. We included a 5% systematic uncertainty in the fits. Best-fit parameters for acceptable models are in Table 3.

An absorbed powerlaw spectrum (wabs*powerlaw) is rejected, with a value of reduced chi-squared statistic $\chi_\nu^2=4.12$ for 23 degrees of freedom (dof), with a null-hypothesis probability of 10^{-10} . The power-law spectrum over-predicts counts in the 2-4 keV range, and under-predicts them in the 4-9 keV range. An absorbed blackbody spectrum is also statistically rejected ($\chi_\nu^2 = 21.4$ for 23 dof).

We find a moderately acceptable fit ($\chi_\nu^2=1.35$) for an absorbed thermal bremsstrahlung spectrum. An absorbed disc blackbody spectrum produces a better fit to the data ($\chi_\nu^2=0.95$), with an

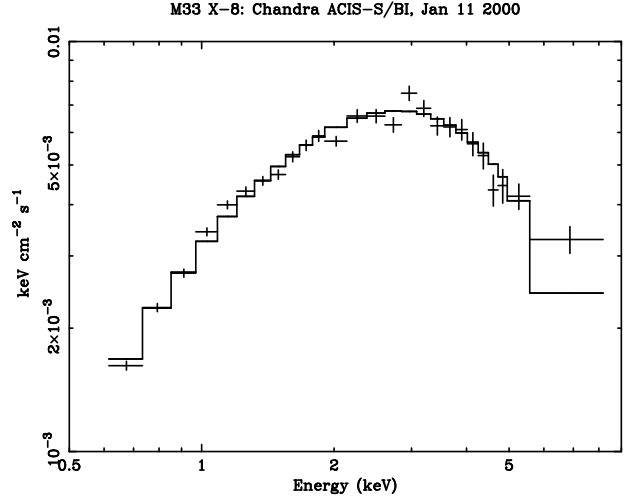


Figure 3. Best-fit absorbed disc-blackbody model (solid-line histogram), with the observed *Chandra*/ACIS-S spectrum of M33 X-8 (crosses), corrected for the detector response, in νF_ν . The deviation of the data points near 3 keV from the model are not significant (2σ); the excess near 6-9 keV deviates from the best-fit model at the 3σ level, and is consistent with possible contributions from pile-up at the $\sim 1\%$ level, which are not accounted for in the best-fit spectrum.

Table 3. *Chandra* Observation Spectral Parameters (0.6-9 keV)

Thermal Bremsstrahlung	
N_H (10^{22}cm^{-2})	0.19 ± 0.01
kT	$3.5 \pm 0.1 \text{ keV}$
$\int n_e n_I dV$	$(1.74 \pm 0.05) \times 10^{62} \text{ cm}^{-3}$
χ_ν^2 (dof)	1.35 (23)
Disc Blackbody	
N_H (10^{22}cm^{-2})	0.06 ± 0.01
T_{in}	$1.18 \pm 0.02 \text{ keV}$
$R_{\text{in}} \sqrt{\cos \theta}$	$57 \pm 3 \text{ km (D/795 kpc)}$
χ_ν^2 (dof)	0.95 (23)

Assumed source distance $d = 795 \text{ kpc}$. Uncertainties are 1σ .

X-ray column density $N_H = (6 \pm 1) \times 10^{20} \text{ cm}^{-2}$, consistent with galactic absorption only⁴. The disc blackbody inner temperature kT_{in} and inner-radius $R_{\text{in}} \sqrt{\cos \theta}$ are identical to the values found in earlier observations with *ASCA* (Takano et al. 1994) and *BepoSAX* (Parmar et al. 2001). The flux (corrected for absorption) of the best-fit spectrum is $2.0 \times 10^{-11} \text{ erg cm}^{-2} \text{ s}^{-1}$, for a luminosity $1.5 \times 10^{39} \text{ erg s}^{-1}$ (0.5-10 keV), consistent (including spectral uncertainty) with previously measured values. Unlike previous work, a power-law component is not required by the data. When we include a power-law component in addition to the absorbed disc-blackbody model, holding $\alpha = 2$ fixed, the 90% confidence upper-limit for the flux of this component is $1.1 \times 10^{-11} \text{ erg cm}^{-2} \text{ s}^{-1}$.

4 X-RAY VARIABILITY

We examined the data for long-term noise-like time variability. We binned the 27259 counts detected in the full *Chandra* pass band, with 1.04104 sec time resolution, and took a Fourier transform

⁴ W3NH at <http://heasarc.gsfc.nasa.gov/> (Dickey & Lockman 1990)

of the data. With the resulting Fourier components, we obtained a power-density spectrum (PDS; see Lewin et al. 1988 for the use of PDS for broad-band timing analysis) which we rebinned logarithmically. Examination of the resulting PDS shows no evidence of power above that expected from Poisson noise. Modelling the power as a power-law of slope=1 plus a constant (held fixed at the Poisson level) in frequency ($P(\nu) = A\nu^{-1} + C$), we find an upper-limit to the root-mean-square variability of <3% (90% confidence; 0.0001-0.5 Hz).

When we binned the data by a factor of 1, 10 and 100, (in which the average counts per bin are 2.938, 29.4, and 294 counts), we find that the maximum counts per bin was 11, 48 and 330 counts, which is consistent with the maximum number of counts expected from Poisson fluctuations. Thus, we find no evidence for intensity variability on timescales between 1 and 10,000 sec.

5 DISCUSSION

The high luminosity of M33 X-8 is not sufficient to rule out a neutron star X-ray binary since magnetospheric accretion can result in super-Eddington luminosities. This was observed e.g. in the high mass X-ray binaries (HMXBs) SMC X-1 or A0535-66. A HMXB would have been an attractive possibility should M33 X-8 have been associated with the nearby 09III star. The *Chandra* localisation of X-8 rules this out (§2). X-8 could still be a HMXB hiding in the nucleus but this would be surprising since the compactness and spectra of the nucleus make it unlikely that it hosts $> 10M_{\odot}$ stars (Long, Charles & Dubus 2002); a HMXB evolves on the uncomfortably short thermal timescale of the donor star ($< 10^5$ yrs for $M_2 > 10M_{\odot}$); the X-ray spectrum of X-8 is unlike that of typical HMXBs which have flat power laws in the 0.5-10 keV range; and the power spectrum shows no evidence for pulsations.

On the other hand, the X-ray spectrum and absence of short-term X-ray variability below 1 Hz are highly reminiscent of the high or very high states of galactic black hole candidates (Tanaka & Lewin 1995). In both states the spectrum is dominated by a disc blackbody with a weak contribution from a steep power law. The very high state shows 3-10 Hz QPOs with a few % rms superposed on 1-10% rms flat top noise in the 1-10 Hz range. There is little variability in the high state. GRS 1915+105, a microquasar in our Galaxy with a $\sim 14M_{\odot}$ black hole accreting from a $\sim 1.2M_{\odot}$ K giant star (Greiner, Cuby & McCaughrean 2001), also has such soft, low variability states (Belloni et al. 2000). The optical emission from such a system would be lost in the nucleus of M33. Since its discovery in 1992, GRS 1915+105 has been steadily detected with X-ray luminosities around or in excess of 10^{39} erg s $^{-1}$.

The analogy with GRS 1915+105 is even more attractive considering the 0.6 mJy (respectively 0.2 mJy) radio source detected by the VLA at 20 cm (6 cm; Gordon et al. 1999) which we show to be consistent with the ultra-luminous X-ray source (§2.4). GRS 1915+105 has been known to show steady radio emission around 30-50 mJy at 2 cm, framed by powerful ejection episodes where the emission from the relativistic jets becomes $\gtrsim 500$ mJy (Fender et al. 1999). The radio source in M33 is more powerful than that; but a small change in the beaming angle of the jet ($\approx 70^\circ$ from the line-of-sight for GRS 1915+105) could easily increase the observed radio flux. Follow-up observations of the radio source are needed to test this hypothesis.

ACKNOWLEDGMENTS

We gratefully acknowledge use of the Vizier catalogue (CDS, France), of data products from the 2MASS survey, and of archival HST and *Chandra* observations obtained from the STScI and SAO websites.

REFERENCES

- Arnaud K. A., 1996, in *Astronomical Data Analysis Software and Systems V*, eds. Jacoby & Barnes, ASP Conf. Series v101, 17
- Belloni T., Klein-Wolt M., Méndez M., van der Klis M., van Paradijs J., 2000, A&A, 355, 271
- Dickey J. M., Lockman F. J., 1990, ARA&A, 28, 215
- Dubus G., Long K. S., Charles P. A., 1999b, ApJ, 519, L135
- Dubus G., Charles P. A., Long K. S., Hakala P. J., Kuulkers E., 1999a, MNRAS, 302, 731
- Dubus G., Charles P. A., Long K. S., Hakala P. J., 1997, ApJ, 490, L47
- Fender R. P., Garrington S. T., McKay D. J. et al., 1999, MNRAS, 304, 865
- Gebhardt K. et al., 2001, AJ, 122, 2469
- Gordon S. M., Duric N., Kirshner R. P., Miller Goss W., Viallefond F., 1999, ApJS, 120, 247
- Gottwald M., Pietsch W., Hasinger G., 1987, A&A, 175, 45
- Greiner J., Cuby J. G., McCaughrean M. J., 2001, Nature, 414, 522
- Haberl F., Pietsch W., 2001, A&A, 373, 438
- Hog E. et al., 2000, A&A, 355, 27
- Long K. S., Charles P. A., Dubus G., 2002, ApJ, accepted (astro-ph/0112327)
- Long K. S., Charles P. A., Blair W. P., Gordon S. M., 1996, ApJ, 466, 750
- Long K. S., D'Odorico S., Charles P. A., Dopita M. A., 1981, ApJ, 246, L61
- Macri L. M., Stanek K. Z., Sasselov D. D., Krokenberger M., Kaluzny J., 2001b, AJ, 121, 870
- Macri L. M., Stanek K. Z., Sasselov D. D., Krokenberger M., Kaluzny J., 2001a, AJ, 121, 861
- Markert T. H., Rallis A. D., 1983, ApJ, 275, 571
- Mochejska B. J., Kaluzny J., Stanek K. Z., Sasselov D. D., Szentgyorgyi A. H., 2001, AJ, 122, 2477
- Monet D. et al., 1998, USNO-A2.0: A Catalog of Astrometric Standards (Washington: US Nav. Obs.)
- Parmar A. et al., 2001, A&A, 368, 420
- Peres G., Reale F., Collura A., Fabbiano G., 1989, ApJ, 336, 140
- Lewin W.H.G., van Paradijs J., van der Klis M., 1988, Space Science Rev., 46, 273
- Schulman E., Bregman J. N., 1995, ApJ, 441, 568
- Skrutskie M. F. et al., 1997, in *The Impact of Large Scale Near-IR Sky Surveys*, eds. F. Garzon et al., 25 (Dordrecht: Kluwer Academic Publishing Company)
- Takano M., Mitsuda K., Fukazawa Y., Nagase F., 1994, ApJ, 436, L47
- Tanaka Y., Lewin W.H.G., 1995, in *X-ray binaries*, eds. Lewin, van Paradijs & van den Heuvel, chap. 3 (Cambridge: CUP)
- van den Bergh S., 1991, PASP, 103, 609